INTERNATIONAL JOURNAL FOR NUMERICAL METHODS IN FLUIDS
Int. J. Numer. Meth. Fluids 2005; **49**:1193–1212
Published online 1 September 2005 in Wiley InterScience (www.interscience.wiley.com). DOI: 10.1002/fld.1016

A physical, mechanistic and fully coupled hillslope hydrology model

David A. Raff[1,*,†] and Jorge A. Ramírez[2]

[1] *US Bureau of Reclamation, Technical Service Center (D-8530), Denver, CO 80225, U.S.A.*
[2] *Department of Civil Engineering, Colorado State University, Ft. Collins, CO 80523, U.S.A.*

SUMMARY

We present the mathematical development and numerical solution of a new model of flow processes on an infiltrating hillslope. We also present validation and sample applications. The model is a distributed, mechanistic, physically based hillslope hydrologic model. The model describes the small-scale processes associated with overland flow, erosion, and sediment transport on an infiltrating surface and is capable of capturing small-scale variations in flow depth, flow velocities, interactive infiltration, erosion rates, and sediment transport. The model couples the fully two-dimensional hydrodynamic equations for overland flow, the one-dimensional Richards equation for infiltration, and a sediment detachment and transport model. Two simulations are presented highlighting the model's ability to capture and describe the interaction between precipitation, overland flow, erosion and infiltration at very small scales. Results of the two-dimensional simulations indicate the system of equations produces hillslopes possessing characteristics of self-organization as observed in real world systems. Copyright © 2005 John Wiley & Sons, Ltd.

KEY WORDS: shallow water equations; Richards infiltration; erosion/sedimentation; hillslope evolution

1. INTRODUCTION

Hydrologists only are constantly faced with problems involving predictions of rainfall-runoff response and sediment production. These problems occur at all scales from point to continental scales. Predictions are often made using lumped hydrologic models, which have traditionally made kinematic wave assumptions. Models based on the governing equations of hillslope hydrology and hydraulics are necessary to fully explain the fine scale processes and

*Correspondence to: David A. Raff, Bureau of Reclamation, Flood Hydrology Group (D-8530), P.O. Box 25007, Denver, CO 80225, U.S.A.
†E-mail: draff@do.usbr.gov

Contract/grant sponsor: Centre for Geoscience/Atmospheric Research; contract/grant numbers: DAAD19-02-2-0005, DAAD19-01-2-0018
Contract/grant sponsor: National Science Foundation Trainee; contract/grant number: 9354864

Received 13 May 2004
Revised 9 May 2005
Accepted 10 May 2005

mechanisms active on hillslopes during precipitation. As knowledge of the small-scale variations in soil properties, topography, flow-depths and velocities increases, modellers have begun to use more complex models to describe these processes and associated interactions. Fiedler and Ramírez [1] developed a 2-D, fully hydrodynamic, mathematical model for simulating the small-scale processes associated with overland flow on an infiltrating surface. Their model is capable of capturing the small-scale variations in flow-depth and velocities and of simulating interactive infiltration. Briefly, the model of Fiedler and Ramírez uses the full hydrodynamic equations (the St. Venant equations in two dimensions) with spatially variable infiltration characteristics and explicit representation of micro topographic features. The hydrodynamic equations are solved using a modified version of the explicit, second-order accurate MacCormack finite difference scheme, with special provisions for small flow depths and a spatially and temporally discontinuous flow regime. Infiltration is modelled with the well-known Green–Ampt equation [2], a good but approximate description of infiltration, which is solved using a standard Newton–Raphson technique.

This paper presents the mathematical development of a new model for hillslope hydrological processes that is largely based on the mathematical model and numerical scheme presented by Fiedler and Ramírez [1]. However, as opposed to the Green–Ampt equation, the new model couples the Richards equation for one-dimensional infiltration to the overland flow equations. The Richards equation is applicable to a wide variety of situations and is easily applied to multi-storm scenarios. The new model also couples a physically based sediment detachment and transport component, which allows examination of the interactions between overland flow, infiltration and sediment detachment and transport. Model numerical results are compared to analytical solutions, and a comparison is made also between a numerical and a physical experiment. Results for a series of two-dimensional simulations are also presented and examined with respect to hillslope evolution and energy expenditure.

2. MATHEMATICAL FORMULATION

2.1. Overland flow

The overland flow component of the new model is a 2-D, fully hydrodynamic, mathematical description of the small-scale processes associated with overland flow on an infiltrating surface and is based on the model of Fiedler and Ramírez [1]. This model allows for explicit representation of micro-topographic features and spatially variable infiltration characteristics. The hydrodynamic equations for overland flow in two dimensions are:

$$\frac{\partial h}{\partial t} + \frac{\partial (uh)}{\partial x} + \frac{\partial (vh)}{\partial y} - q_{\mathrm{l}} = 0 \tag{1}$$

$$\underbrace{\frac{\partial (uh)}{\partial t} + \overbrace{\frac{\partial (u^2 h)}{\partial x} + \frac{\partial (uvh)}{\partial y} + g\frac{\partial (h^2/2)}{\partial x} - \overbrace{gh(S_{\mathrm{o}x} - S_{\mathrm{f}x})}^{\text{kinematic wave}}}^{\text{diffusive wave}}}_{\text{dynamic wave}} - \overbrace{uq_{\mathrm{l}}}^{\text{lateral}} = 0 \tag{2}$$

$$\frac{\partial(vh)}{\partial t} + \frac{\partial(v^2h)}{\partial y} + \frac{\partial(uvh)}{\partial x} + g\frac{\partial(h^2/2)}{\partial y} - gh(S_{oy} - S_{fy}) - \overbrace{vq_l}^{\text{lateral}} = 0 \tag{3}$$

where h [L] is flow depth, u and v are velocities [L/T] in the x and y directions, respectively, S_o is bed slope [L/L] and S_f is energy grade line slope (or friction slope) [L/L], and q_l is lateral flux [L^2/T] through the control boundary and is equal to the difference between precipitation and infiltration. It has been shown that the kinematic wave approximation is only appropriate in very small regions of hydraulic roughness and Froude numbers and that the diffusive and quasi-steady dynamic wave approximations are not appropriate for supercritical overland flow [3]. It is therefore desirable to implement the full dynamic-wave form of the momentum equations for an accurate representation of spatially and temporally variable overland flow. The bed slopes, S_{ox} and S_{oy} are computed directly from ground surface elevations, z, as

$$S_{ox} = -\frac{\partial z}{\partial x} \quad \text{and} \quad S_{oy} = -\frac{\partial z}{\partial y} \tag{4}$$

respectively. The Darcy–Weisbach (D–W) formula is used to compute the friction slopes, S_{fx} and S_{fy} as

$$S_{fx} = \frac{f}{8g}\frac{p\sqrt{(p^2+q^2)}}{h^3} \quad \text{and} \quad S_{fy} = \frac{f}{8g}\frac{q\sqrt{(p^2+q^2)}}{h^3} \tag{5}$$

respectively, where p and q are fluxes [L^2/T] in the x and y directions, respectively. The value f is the D–W friction factor and, assuming that the overland flow regime is laminar [4], it is calculated as

$$f = \frac{K_0}{R_e} \tag{6}$$

a function of the Reynolds number

$$R_e = \frac{\sqrt{(p^2+q^2)}}{v} \tag{7}$$

and K_0 a constant related to the characteristics of the ground surface [5], and v is the kinematic viscosity of water. The kinematic viscosity of the sediment water mixture, v_m, is a function of the sediment concentration as

$$v_m = \frac{\mu_m}{\rho_m} \tag{8}$$

where ρ_m is the density of the mixture, μ_m is the dynamic viscosity of the sediment water mixture determined from an empirical equation [6]

$$\mu_m = \mu(1 + 2.5C_v) \tag{9}$$

and C_v is the sediment concentration by volume. For details on numerical methods used for solutions of the overland flow equations the reader is directed to the work of Fiedler and Ramírez [1].

2.2. Infiltration

2.2.1. Governing equations. The governing equation for one-dimensional flow of water in soil can be written in the form

$$\frac{\partial}{\partial z_g}\left(K(\psi)\frac{\partial \psi}{\partial z_g}\right)+\frac{\partial K(\psi)}{\partial z_g}=\frac{\partial \theta(\psi)}{\partial t} \tag{10}$$

a second-order cubic partial differential equation commonly referred to as the mixed form of the Richards equation, where ψ is the soil water pressure head, $\theta(\psi)$ is the soil volumetric water content, $K(\psi)$ is the hydraulic conductivity and z_g denotes a length scale directed parallel with the gravity vector. Two other common forms of Richards equation are the head- and the theta-based forms in which all the gradients are of ψ and θ, respectively. While each form of Richards equation has been used extensively throughout the literature [7–9] the mixed form has been chosen here because its numerical implementation has been shown to be perfectly mass conservative and solutions based on the head- or theta-based forms generally yield poor results specifically due to large mass balance errors [7]. Because of its complex non-linear nature, there is no known general analytical solution to the Richards equation for water flow in an unsaturated soil column.

2.2.2. Numerical methods. Following the work of Celia *et al.* [7], a fully implicit finite difference scheme coupled with a simple one-step Euler time-marching algorithm is used here to solve the mixed form of Richards equation. The solution uses the Picard method for the iteration procedure of the linearized system of non-linear equations that result from discretizing Richards equation. The backward Euler approximation of Equation (10) is

$$\frac{\theta^{n+1,m+1}-\theta^{n,m}}{\Delta t}-\frac{\partial}{\partial z_g}\left(K^{n+1,m}\frac{\partial \psi^{n+1,m+1}}{\partial z_g}\right)-\frac{\partial K^{n+1,m}}{\partial z_g}=0 \tag{11}$$

where superscripts n and m denote time and iteration level, respectively. The mass balance accuracy of the numerical solution of the mixed form of Richards equation comes from the expansion of $\theta^{n+1,m+1}$ in a truncated Taylor series with respect to ψ, about the expansion point $\psi^{n+1,m}$

$$\theta^{n+1,m+1}=\theta^{n+1,m}+\left.\frac{\mathrm{d}\theta}{\mathrm{d}\psi}\right|^{n+1,m}(\psi^{n+1,m+1}-\psi^{n+1,m})+O[(\delta^m)^2] \tag{12}$$

Substituting a first-order approximation of Equation (12) into Equation (11) and an iteration increment $\delta^m=\psi^{n+1,m+1}-\psi^{n+1,m}$ results in

$$\left(\frac{1}{\Delta t}C^{n+1,m}\right)\delta^m-\frac{\partial}{\partial z_g}\left(K^{n+1,m}\frac{\partial \delta^m}{\partial z_g}\right)=\frac{\partial}{\partial z_g}\left(K^{n+1,m}\frac{\partial \psi^{n+1,m}}{\partial z_g}\right)+\frac{\partial K^{n+1,m}}{\Delta z_g}-\frac{\theta^{n+1,m}-\theta^{n,m}}{\Delta t} \tag{13}$$

where $C=\mathrm{d}\theta/\mathrm{d}\psi$.

Equation (13) has been called the general mixed-form Picard approximation by Zarba [10]. Using finite differences results in the final discrete form of the approximation [7]

$$\left\{C_i^{n+1,m}\frac{\delta_i^m}{\Delta t}-\frac{1}{(\Delta z_g)^2}[K_{i+1/2}^{n+1,m}(\delta_{i+1}^m-\delta_i^m)-K_{i-1/2}^{n+1,m}(\delta_i^m-\delta_{i-1}^m)]\right\}$$

$$= \left\{ \frac{1}{(\Delta z_g)^2} \left[K_{i+1/2}^{n+1,m} (\psi_{i+1}^{n+1,m} - \psi_i^{n+1,m}) - K_{i-1/2}^{n+1,m} (\psi_i^{n+1,m} - \psi_{i-1}^{n+1,m}) \right] \right.$$

$$\left. + \frac{K_{i+1/2}^{n+1,m} - K_{i-1/2}^{n+1,m}}{\Delta z_g} - \frac{\theta_i^{n+1,m} - \theta_i^{n,m}}{\Delta t} \right\} \tag{14}$$

Equation (14) is appropriate for all interior nodes. Boundary conditions must be specified at $i = 0$ and $N - 1$ where N is the number of nodes. Boundary conditions can be of two types, either fixed head or flux type. With fixed head boundary conditions there are $N - 2$ equations with $N - 2$ unknown values of δ^m. The form of these $N - 2$ equations is such that they can be put into a matrix equation with a dominant tri-diagonal matrix

$$\begin{bmatrix} b_1 & c_1 & 0 & \dots & & & \\ a_2 & b_2 & c_2 & \dots & & & \\ & & & \dots & & & \\ & & & \dots & a_{N_n-1} & b_{N_n-1} & c_{N_n-1} \\ & & & \dots & 0 & a_{N_n} & b_{N_n} \end{bmatrix} \cdot \begin{bmatrix} u_1 \\ u_2 \\ \dots \\ u_{N_n-1} \\ u_{N_n} \end{bmatrix} = \begin{bmatrix} R_1 \\ R_2 \\ \dots \\ R_{N_n-1} \\ R_{N_n} \end{bmatrix} \tag{15}$$

where $N_n = N - 2$, and from expanding Equation (14)

$$a_i = -\frac{1}{(\Delta z_g)^2} K_{i+1/2}^{n+1,m} \tag{16}$$

$$b_i = C_i^{n+1,m} \frac{1}{\Delta t} + K_{i-1/2}^{n+1,m} \frac{1}{(\Delta z_g)^2} + K_{i+1/2}^{n+1,m} \frac{1}{(\Delta z_g)^2} \tag{17}$$

$$c_i = -\frac{1}{(\Delta z_g)^2} K_{i-1/2}^{n+1,m} \tag{18}$$

$$u_i = \delta_i^m \tag{19}$$

$$R_i = \frac{1}{(\Delta z_g)^2} [K_{i+1/2}^{n+1,m} (\psi_{i+1}^{n+1,m} - \psi_i^{n+1,m}) - K_{i-1/2}^{n+1,m} (\psi_i^{n+1,m} - \psi_{i-1}^{n+1,m})]$$

$$+ \frac{K_{i+1/2}^{n+1,m} - K_{i-1/2}^{n+1,m}}{\Delta z_g} - \frac{\theta_i^{n+1,m} - \theta_i^{n,m}}{\Delta t} \tag{20}$$

R_i is a measure of the error associated with the current iteration level and approaches zero along with all values of δ^m as the solution converges. This matrix system can be solved using a **LU** decomposition technique; a specific solution can be found in Reference [11].

For a flux boundary condition at $i = 0$ there are $N - 1$ equations and $N - 1$ values of δ^m where the interior nodes are described by Equation (4) and the boundary at $i = 0$ is described

by Darcy's Law. This set of equations can be solved exactly as above where $N_n = N - 1$ and a_1 is described through Darcy's Law.

In order to couple the above infiltration model to the overland flow equations, the solution approach of Reference [7] requires two modifications. First, because of erosion and sediment transport processes (presented below), ground surface elevations are not constant in general, and, therefore the soil column is not generally static. Thus, new node vectors must be defined at each time step. Redefining the node vector is accomplished by changing Δz_g while maintaining the same number of nodes in each soil column. This is a source of error; however, because the amount of erosion/deposition at a time step is much less than Δz_g, this error is relatively small. The second modification to the approach of Reference [7] incorporates the ability to switch boundary conditions. When rainfall starts, the boundary condition is a flux type such that the flux is equal to the rainfall rate plus the flow onto each cell from adjacent cells. When the head value in the uppermost node becomes greater than the saturated head, ponding occurs and the boundary condition at that cell switches to a fixed head type with the head equal to the saturated head value.

2.3. Sediment detachment and transport

2.3.1. Governing equations. Conservation of sediment for a three-dimensional control volume gives

$$\frac{\partial C_s}{\partial t} + \frac{\partial \hat{q}_{s_x}}{\partial x} + \frac{\partial \hat{q}_{s_y}}{\partial y} + \frac{\hat{\partial} q_{s_z}}{\partial z} = \dot{C}_s \tag{21}$$

where C_s is the spatially averaged sediment concentration, $\hat{q}_{s_x}, \hat{q}_{s_y}$ and $\hat{q}_{s_z}$ are the sediment mass fluxes through the faces of the control volume in the x, y, and z directions, respectively, and $\dot{C}_s$ is the sink/source term as a rate of sediment per unit volume. Assuming that the sediment concentration is gradually varied (i.e. $\partial C_s/\partial t = 0$), Equation (21) reduces to

$$\frac{\partial \hat{q}_{s_x}}{\partial x} + \frac{\partial \hat{q}_{s_y}}{\partial y} + \frac{\hat{\partial} q_{s_z}}{\partial z} = \dot{C}_s \tag{22}$$

The sediment mass flux through each face includes advective flux and both molecular and turbulent diffusive fluxes, and can be written as

$$\begin{aligned} \hat{q}_{s_x} &= \overbrace{uC_s}^{\text{advective flux}} - \overbrace{(D + \varepsilon_x)\frac{\partial C_s}{\partial x}}^{\text{diffusive and mixing flux}} \\ \hat{q}_{s_y} &= vC_s - (D + \varepsilon_y)\frac{\partial C_s}{\partial y} \\ \hat{q}_{s_z} &= \omega C_s - (D + \varepsilon_z)\frac{\partial C_s}{\partial z} \end{aligned} \tag{23}$$

The advective flux describes the movement of sediment particles by velocity currents where u, v, and ω in Equation (23) are the velocity of the sediment flux in the x, y, and z directions, respectively. The diffusive and mixing fluxes are directly proportional to the concentration gradient and correspond to molecular diffusion (D) and to diffusion due to turbulent fluid motion ($\varepsilon_x, \varepsilon_y, \varepsilon_z$). The negative sign in Equation (23) represents a mass flux in the direction

of decreasing concentration. Assuming that the diffusive and mixing fluxes are negligible compared to advective fluxes and that settling velocity, ω_z, is the dominant advective flux in the z direction, Equation (22) can be written as

$$\frac{\partial uC_s}{\partial x} + \frac{\partial vC_s}{\partial y} - \frac{\partial \omega_z C_s}{\partial z} = \dot{C}_s \tag{24}$$

For conditions where the sediment transport is capacity-limited (as opposed to supply-limited), the sediment mass fluxes are equal to the sediment transport capacities of the flow. The unit sediment transport capacity in the x direction (and analogously for the other directions) is defined by

$$q_{s_x} = \eta[pS_{0x} - (pS_0)_{crit}]^{\xi} \tag{25}$$

where S_{ox} is the bed slope in the x direction of flow and $(pS_0)_{crit}$ is a minimum value below which no sediment is transported. The parameter η is a measure of the erodability of the sediment and the parameter exponent ξ is generally in the range 1.5–1.8 [12]. Assuming that the sediment mass flux is uniform in the vertical ($\partial \omega_z C_s/\partial z = 0$), Equation (24) becomes

$$\frac{\partial q_{s_x}}{\partial x} + \frac{\partial q_{s_y}}{\partial y} = \dot{C}_s \tag{26}$$

The volumetric flux rate of sediment either deposited to or eroded from the bed causes a change in bed elevation and is

$$\dot{C}_s = -\frac{\partial}{\partial t}[(1 - p_o)z] \tag{27}$$

where p_o is the bed porosity (fraction of bed volume that is pores rather than sediment). In its current implementation the model utilizes only one size class of sediment and p_o is determined by the specific weight of the sediment as

$$p_o = 1 - \frac{\gamma_{md}}{\gamma_s} \tag{28}$$

where γ_{md} is the average dry specific weight of the water–sediment mixture, defined here as the dry weight of sediment per unit total volume, and γ_s is the specific weight of the sediment [6]. Substituting (27) into (26) results in

$$-(1 - p_o)\frac{\partial z}{\partial t} = \frac{\partial q_{s_x}}{\partial x} + \frac{\partial q_{s_y}}{\partial y} \tag{29}$$

which can be rewritten in the form of the well known Exner equation

$$\frac{\partial z}{\partial t} = -\frac{1}{(1 - p_o)}\left(\frac{\partial q_{s_x}}{\partial x} + \frac{\partial q_{s_y}}{\partial y}\right) \tag{30}$$

This is the governing equation for bed elevation change as a function of changes in sediment load.

2.3.2. Numerical methods. The sediment detachment and transport equations are solved using a finite difference method, centred in space, forward in time. Because the coupling of the erosion and sedimentation algorithm to the overland flow equations can cause steep gradients in flow conditions and bed slope, which can lead to discretization errors, a simple Gaussian low-pass filter is applied to the bed elevation after each time the sediment detachment and transport algorithm is implemented. The Gaussian distribution in 2-D for an isotropic, zero mean variable with variance σ^2 is given by

$$G(x, y) = \frac{1}{\sqrt{2\pi\sigma^2}} \, \mathrm{e}^{-(x^2+y^2)/2\sigma^2} \tag{31}$$

The Gaussian filter gives a 'point-spread' function where each cell's new elevation is determined by its own value and the elevations of the cells within a neighbourhood of dimensions specified in the input. This filter is applied to every cell in the domain to determine the bed elevation values for the next time step. The variance of the distribution, σ^2, is the relative convolution weight in determining elevation values and it is assumed constant in the x and y directions.

3. MODEL COMPONENT VERIFICATION

3.1. Overland flow

The overland flow component was extensively tested when originally presented by Fiedler and Ramírez [1] using the Green–Ampt infiltration model. Internal validation was performed testing the model with an analytical solution to a kinematic wave [13] as well as a dam break problem [14, 15]. The reader is kindly referred to Fiedler and Ramírez for details.

3.2. Infiltration

3.2.1. Numerical accuracy. To test the numerical accuracy of the infiltration model implementation, model results are compared to a quasi-analytical solution of Richards equation for the condition of a homogeneous soil column with a fixed head boundary condition presented by Philip [16]. Results from only one simulation corresponding to a yolo light clay soil column are presented; the model produced similar accuracy during tests for other soil types. The soil properties for the yolo light clay are defined as follows [17]:

Yolo light clay:

$$\begin{aligned} K(\psi) &= K_s \frac{A}{A + |\psi|^\beta}; \quad K_s = 4.428(10^{-2})\,\mathrm{cm/h}, \quad A = 124.6, \quad \beta = 1.77 \\ \theta(\psi) &= \frac{\alpha(\theta_s - \theta_r)}{\alpha + (\ln|\psi|)^\beta} + \theta_r; \quad \theta_s = 0.495, \quad \theta_r = 0.124, \quad \alpha = 739, \quad \beta = 4 \end{aligned} \tag{32}$$

Figure 1 shows the comparison between the theoretical and analytical solutions. As can be seen, the numerical solution of the Richards equation does an excellent job of simulating the results of the quasi-analytical solution for this specific case of the distribution of water in the soil column.

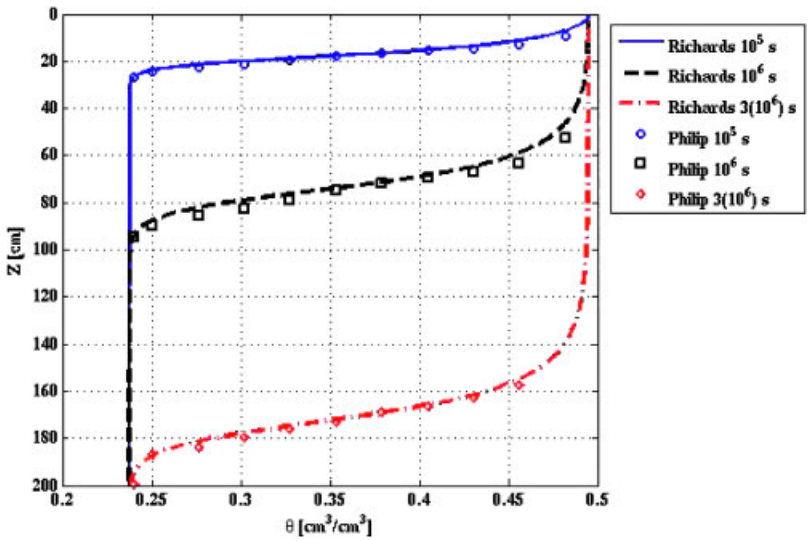

Figure 1. Theoretical and analytical solution for infiltration into yolo light clay.

3.2.2. Mass balance. The mass balance (MB) ratio is defined as the ratio of the total additional mass in the domain to the total net flux into the domain, and is written as

$$\mathrm{MB} = \frac{\sum_{i=1}^{E-1} (\theta_i^{n+1} - \theta_i^0)(\Delta z)}{\sum_{j=1}^{n+1} \left[K_{N-1/2}^j \left(\frac{\psi_N^j - \psi_{N-1}^j}{\Delta z} + 1 \right) - K_{1/2}^j \left(\frac{\psi_1^j - \psi_0^j}{\Delta z} + 1 \right) \right] (\Delta t)} \tag{33}$$

where $N = E + 1$ nodes $\{z_0, z_1, z_2, \ldots, z_E\}$, and constant nodal spacing Δz is assumed.

In the numerical experiment as presented in Figure 1 the mass balance ratio is unity. This is a result of the utilization of the mixed form of Richards equation and the numerical implementation used here as it has been shown to be perfectly mass conservative [7].

3.3. Sediment detachment and transport

Since there is no known analytical solution to the coupled erosion and overland flow equations being implemented here, it is impossible to perform an analytical verification of this component. However, an empirical test is feasible based on expected characteristics of surface elevations, for example the longitudinal profile. This was done for a 10 m long plane with initial longitudinal slope of 0.008 and constant rainfall rate of 105 mm/h and using $\Delta_x = \Delta_y = 0.0625$ m. The sediment transport parameters are set as $\eta = 50$ and $\xi = 1.8$ and $(pS_{ox})_{\mathrm{crit}} = (qS_{oy})_{\mathrm{crit}} = 5(10^{-7})\,\mathrm{cm}^2/\mathrm{s}$. The diameter of the sediment particles is set to 0.12 mm.

Figure 2 shows the temporal progression of the longitudinal profile of the landform to a near equilibrium condition that is best described using an exponential function with a negative exponent, a result that is consistent with expected longitudinal profiles [18].

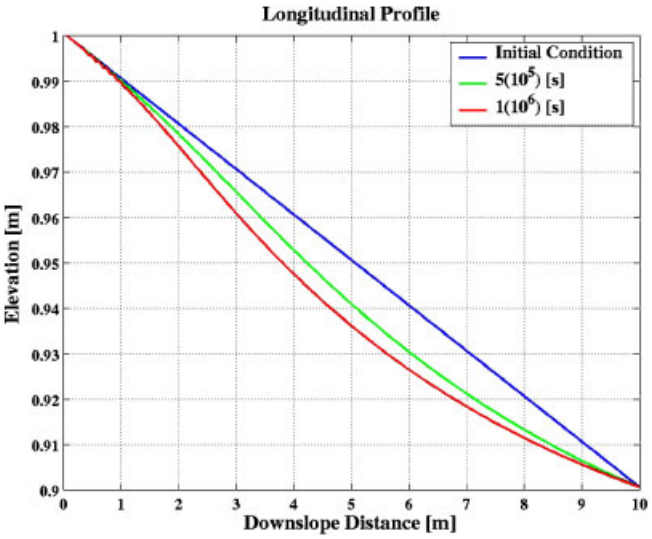

Figure 2. Theoretical longitudinal profile development.

3.4. *Physical/theoretical model comparison*

A physical experiment was conducted in an experimental rainfall facility located at the Hydraulics Laboratory at Colorado State University to test the theoretical model's ability to model an actual rainfall-runoff event. The experimental facility consists of a rainfall simulator and a 1 m × 0.5 m partitioned section of an artificial hillslope [19] with a 5° slope angle. The experiment subjected the hillslope to a mean rainfall rate of approximately 65 mm/h, applied in two 25-min pulses separated by a 5-min time period of no rain. Measurements of volumetric water flux [L^3/T] were made at intervals of 120 s. The hydraulic conductivity and the water pressure head for the soil of the physical model are given by the van Genuchten functions:

$$K(\psi) = K_s S_e^{0.5}[1 - (1 - S_e^{1/f})^f]^2 \tag{34}$$

$$S_e = \frac{\theta(\psi) - \theta_r}{\theta_s - \theta_r} = \frac{1}{[1 + |\alpha\psi|^w]^f} \tag{35}$$

where $f = 1 - 1/w$. The values of θ_s, θ_r, K_s, α and w are best fits to laboratory measurements and obtained as, $\theta_s = 0.42, \theta_r = 0.04, K_s = 0.0004$ cm/s, $\alpha = 0.0436$ cm^{-1}, and $w = 1.34$.

The theoretical model is parameterized with the above van Genuchten functions and the initial soil moisture condition is assumed characterized by a soil matric potential $\psi = -10$ cm everywhere in the domain, a value consistent with the volumetric water content after 1 day of drying [19] following a rainfall of 1 h duration. The model was discretized with $\Delta_x = \Delta_y =$ 50 mm and a time step of 0.02 s was utilized. The model was run continuously for a period of 3600 s with a rainfall field distributed spatially to correspond to measurements from the physical model [19]. A comparison of hydrographs can be seen in Figure 3. The theoretical

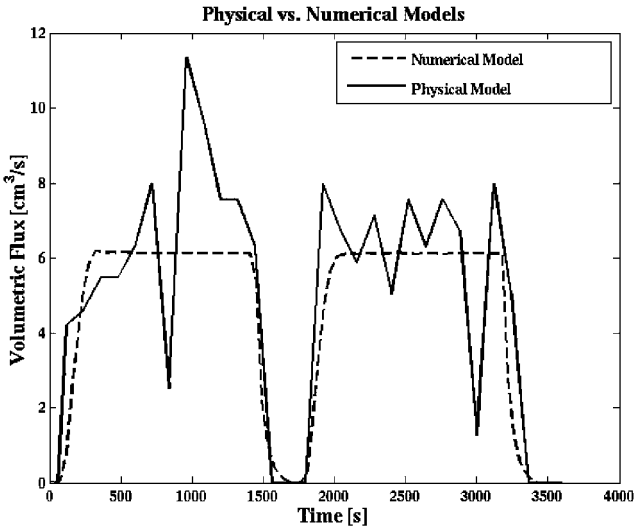

Figure 3. Model verification with physical experiment.

model reproduces very well the rising and falling limbs of the runoff response to both pulses of rain. This is an advantage of implementing the Richards equation because using a different infiltration equation such as Green–Ampt requires additional parameterization for a multi-storm event [20]. The total volumetric runoff of the physical experiment and theoretical model are 18.4 and 17.4 l, respectively. This represents a 5.6% error. Large-scale oscillations, however, which can be of the same order as the signal in the physical experiment, are not reproduced in the theoretical model. During the physical experiment mass-wasting events dam the outflow until the water behind the dam becomes deep enough to over top the dam and move the sediment. A pulsed outflow is observed due to this dam and release process and can be seen in the physical results. There is no mass-wasting mechanism implemented in the theoretical model and therefore this pulsed outflow type of event cannot be reproduced exactly.

4. SAMPLE SIMULATIONS

4.1. Initial conditions

One of the advantages of the mathematical model developed and implemented here is that physical characteristics of the hillslope may be explicitly defined at each grid cell, namely rainfall rates, elevation, soil infiltration characteristics (e.g. saturated hydraulic conductivity), soil erodability, etc. In order to study how the governing equations control hillslope evolution with respect to energy expenditure, initial soil moisture distribution and erodability are assumed constant throughout the domain. The hillslope is initially completely smooth. Variability into the system is introduced by spatially variable rainfall rate. Two experiments are presented; the first two-dimensional test (DD1) has cell dimensions $\Delta_x = \Delta_y = 6.25$ mm and the second (DD3) has cell dimensions $\Delta_x = \Delta_y = 3.125$ mm. Domain size for the two simulations is $3\,\text{m} \times 10\,\text{m}$.

Model parameters are set to resemble those of the physical model in the experimental rainfall facility. A grain size of 0.12mm is selected to correspond with median grain size of the physical model [19]. Initial slope angle is 9°. The sediment transport capacity is parameterized as to allow for rapid sediment transport: $\eta = 50, \xi = 1.8, (pS_{ox})_{\text{crit}} = (qS_{oy})_{\text{crit}} = 5(10^{-7})\,\text{cm}^2/\text{s}$. Model stability requires that a time step be selected such that the Courant condition is met and that the change in elevation at a cell at any time step is not greater than 5% of the flow depth. Time steps are 10^{-3} s.

A summary of the two simulations is presented in Table I. Experiment DD1 corresponds to a self-similar distribution of rainfall rates with mean and variance of 85 mm/h and 496 $(\text{mm/h})^2$, respectively. The distribution of rainfall rates corresponds to a power function semi-variogram ($g = ar^{\beta}$) where g is half the variance between points located distance r apart. For this distribution a is set to 1 and β is set to 1.5, which yields a fractal dimension of 2.25 (Figure 4). Experiment DD3 corresponds to a Gaussian rainfall distribution whose mean and variance are 59 mm/h and 25 $(\text{mm/h})^2$, respectively, and whose correlation length scales are 600 mm in the x-direction and 800 mm in the y-direction (Figure 5).

Table I. Theoretical model simulation characteristics.

Experiment ID	Mean rainfall rate mm/h	Standard deviation rainfall rate	$\Delta_x; \Delta_y$ mm	$N_x; N_y$	Rainfall distribution
DD1	85	22	6.25; 6.25	48; 160	Self-similar Figure 4
DD3	59	5	3.125; 3.125	96; 320	Gaussian Figure 5

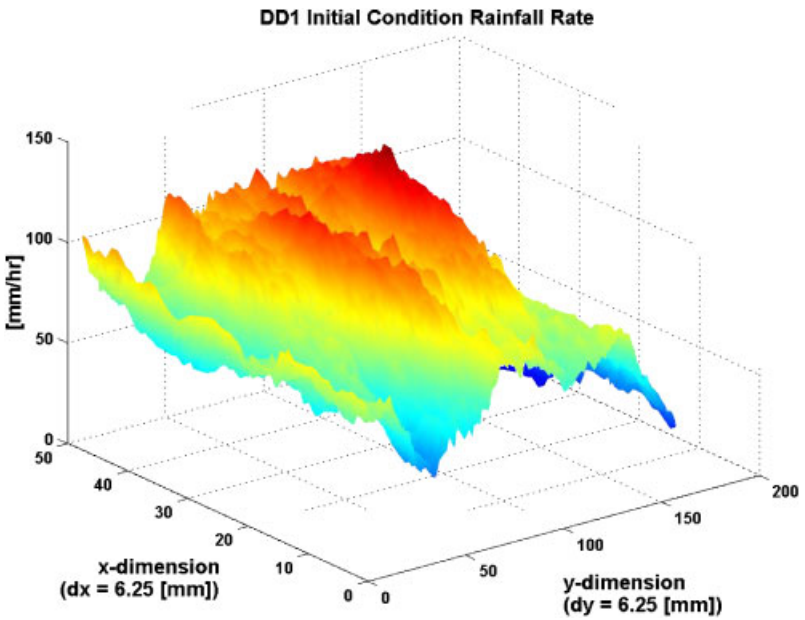

Figure 4. Self-similar rainfall rate distribution for simulation DD1.

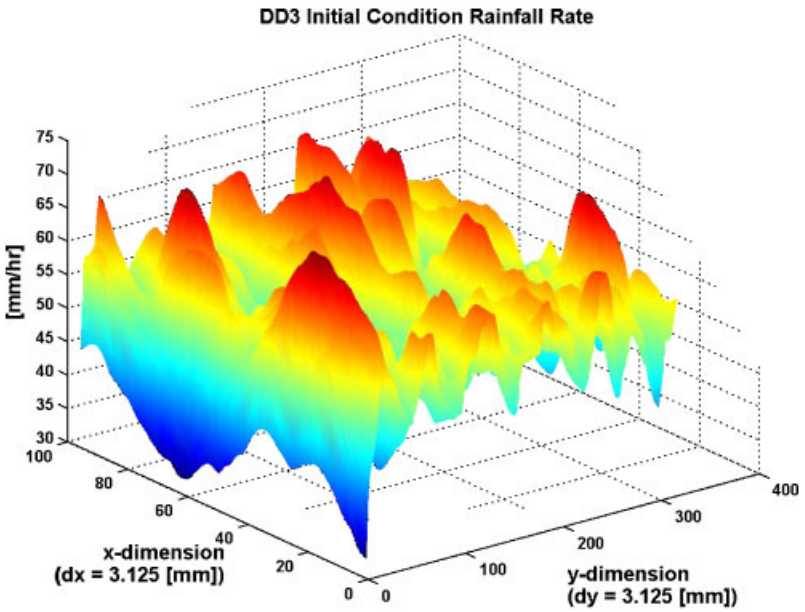

Figure 5. Gaussian rainfall rate distribution for simulation DD3.

As with all numerical solutions of hyperbolic partial differential equations, these solutions are prone to numerical oscillations. In addition, the implementation of the erosion and sediment transport component can also cause oscillations in the solution. Experimentally, it was found that these oscillations are best controlled through Gaussian smoothing (Section 2.3.2), and through adjustments of the grid size and time steps. In particular, a time step adjustment proved to be very successful. Operating the erosion algorithm at a time step, $\Delta t_e > 3\Delta t_o$ (where Δt_o is the time step for overland flow algorithm) provides stability under applications tested during the experiments described in this manuscript.

4.2. Two-dimensional simulation results

Results from two-dimensional simulations of an initially smooth slope subject to spatially variable rainfall rates are very complex. The scales at which the system is in adjustment vary in both space and time. Some sample flow domain plots are shown in Figures 6 and 7. Under the initial and boundary conditions specified for these two examples (see Table I), it is clear that the down slope component of discharge is initially dominant in both cases; however, with time, the cross-slope component of discharge can become of equal magnitude (Figures 6 and 7).

Examinations of the energy expenditure characteristics of the simulated flow domains show evidence of two-dimensional self-organization with time. The energy expenditure characteristics analysed are: cell-based global energy expenditure, coefficient of variation of energy expenditure, total stream power and unit stream power and are defined below.

Unit stream power is defined as [21]

$$\zeta = vS \tag{36}$$

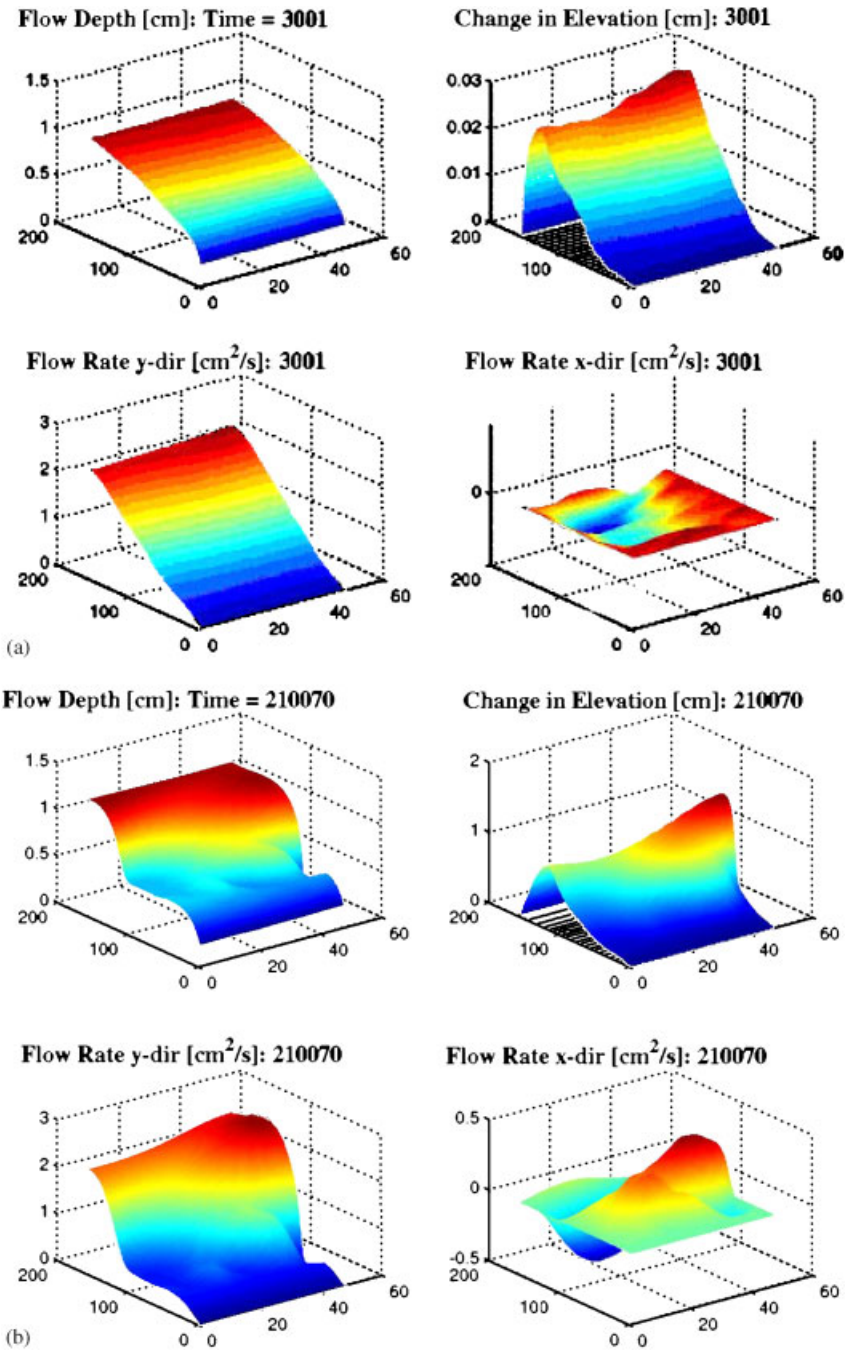

Figure 6. Sample flow domain (DD1): (a) Time = 3001 s; (b) Time = 210 000 s.

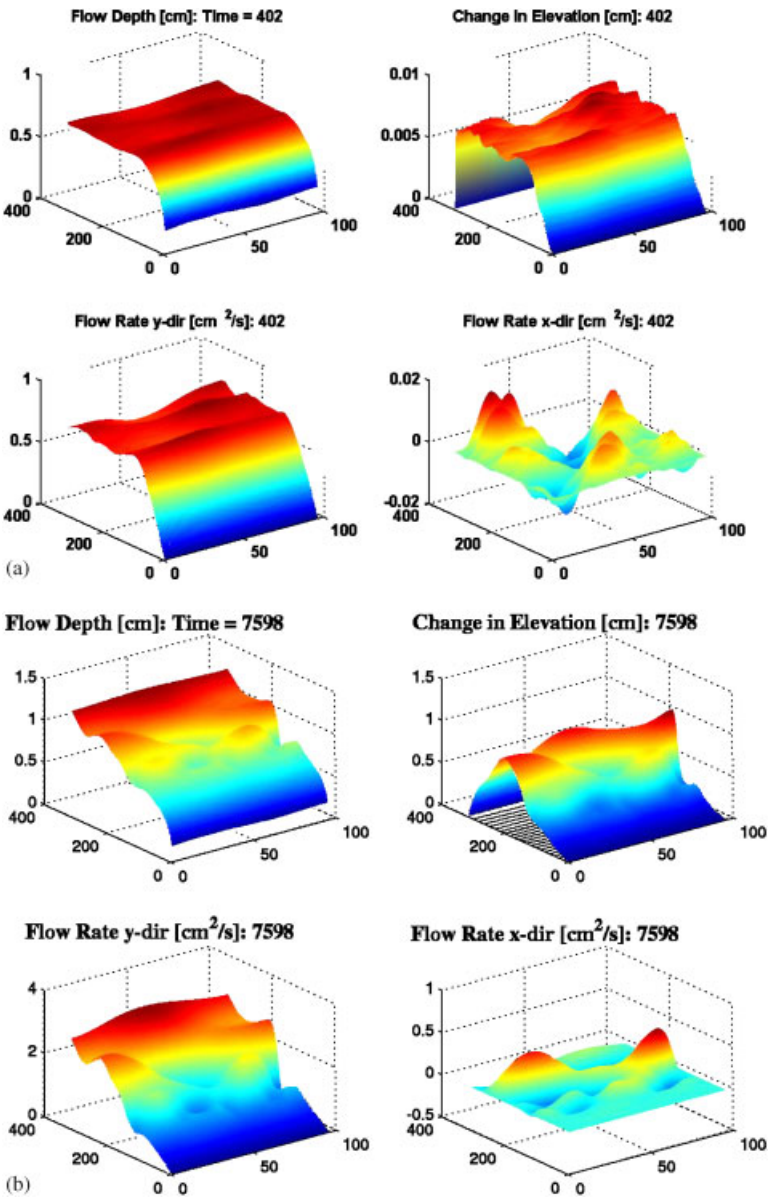

Figure 7. Sample flow domain (DD3): (a) Time = 402 s; (b) Time = 7598 s.

where v is velocity, and S is slope. Application of the concept of unit stream power to these simulations where the flow domain may be continuous across the entire hillslope requires unit stream power at a point i, j to be defined as

$$\zeta_{i,j} = v_{i,j} S_{i,j} \tag{37}$$

and the total unit stream power in the system as

$$\zeta_T = \sum_{i=1}^{Nx} \sum_{j=1}^{Ny} v_{i,j} S_{i,j} \tag{38}$$

where $i \in (1{:}N_x)$ and $j \in (1{:}N_y)$ and N_x and N_y are the number of grid cells in the x and y directions, respectively. Stream power per unit length is defined as [22]

$$\Omega = \gamma Q S \tag{39}$$

Again defined here for a continuous domain, stream power at a point i, j is

$$\Omega_{i,j} = \gamma_{\mathrm{m}i,j} Q_{i,j} S_{i,j} \tag{40}$$

where $\gamma_{\mathrm{m}i,j}$ is the specific weight of the sediment water mixture and can be calculated as

$$\gamma_{\mathrm{m}i,j} = \gamma(1 + C_{\mathrm{v}}(G - 1)) \tag{41}$$

where G is the specific gravity of the sediment and C_{v} is the concentration of sediment by volume. Here, for simplicity in calculations, it is assumed that $\gamma_{\mathrm{m}i,j}$ is a constant in space and time. The total stream power in the system is thus

$$\Omega_{\mathrm{T}} = \gamma \sum_{i=1}^{Nx} \sum_{j=1}^{Ny} Q_{i,j} S_{i,j} \tag{42}$$

Making similar arguments when developing characterization of global and local energy expenditure for a continuous flow domain transporting sediment, the global rate of energy expenditure of the flow domain is calculated here as

$$P_{\mathrm{T}} = \sum_{i}^{Nx} \sum_{j}^{Ny} Q_{i,j} S_{i,j} L_{i,j} \tag{43}$$

where $L_{i,j}$ is the length of the cell in the direction of flow. The local rate of energy expenditure per unit flow area is computed at each cell as

$$P_{\mathrm{l}} = \frac{QS}{2h + d_x} \tag{44}$$

where h is flow depth at that cell and d_x is the cell dimension along the direction of flow. Equation (44) assumes that the flow is directed in the x direction, but analogous equations may be written regardless of the direction of flow. The coefficient of variation of P_{l} across the entire domain is computed as

$$\mathrm{CV}_{P_{\mathrm{l}}} = \frac{\sigma_{P_{\mathrm{l}}}}{\mu_{P_{\mathrm{l}}}} \tag{45}$$

where $\sigma_{P_{\mathrm{l}}}$ and $\mu_{P_{\mathrm{l}}}$ are the standard deviation and mean of P_{l} across the entire flow domain, respectively.

In natural drainage systems, observations indicate that the local terrain slope at a point, S, is related to the flow discharge passing through that point, Q, by a power law of the form $S \propto Q^{-z}$ [23–25]; furthermore, for so-called optimal channel networks, it can be shown

that $z = 0.5$ [25, 26]. Figure 8 shows the simulated slope-discharge relationship at the end of the DD1 simulation. Within Figure 8, the line in yellow is proportional to $Q^{-0.5}$ and the proportionality factor is selected to fit the data with a minimum sum of square errors. The R^2 value of the fit is 0.48. The thresholds indicated in Figure 8 are used to define areas of concentrated flow for energy expenditure analyses. The higher threshold corresponds to areas where water fluxes and elevation changes are approaching dynamic stability at the end of simulation (as evidenced by slope of the S vs Q relationship approaching optimality) and the lower threshold to areas still in active adjustment. Results of the energy expenditure analysis are presented for DD1 only, similar results were obtained for DD3. Physically, global energy expenditure decreases within the system as a function of time. Energy expenditure as a result of the distributed erosional work being done throughout the domain decreases slope overall ($\partial z/\partial t < 0$). This can be seen by the generally decreasing trend in total stream power and global energy expenditure (Figure 9). The amount of work that can be done in any given time interval is related exponentially to the discharge and slope during that time. Thus, different areas are varying at different rates as can be seen in the plots of the CV_{P_1} as function of the local slope and local discharge (Figure 9), the implication being that networks not in equilibrium do not always have trends in local energy expenditure approaching optimality. The trends of local and global energy expenditure for areas approaching equilibrium resemble those that have been discussed in the literature for optimal channel networks (OCNs) which have been shown to result from models of self-organization [26].

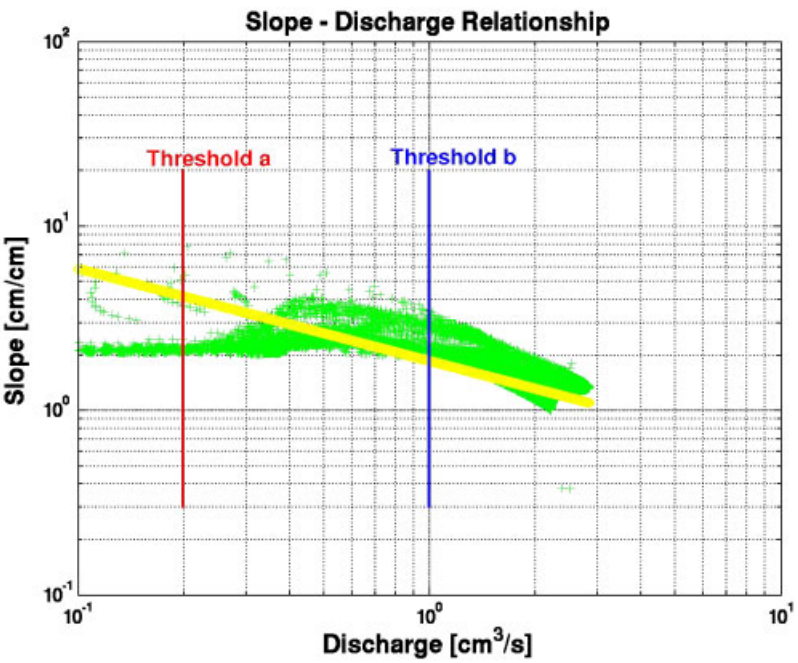

Figure 8. DD1 slope–discharge relationship. Data points are raw slope vs discharge. Line is $S \propto Q^{-0.5}$. Vertical lines are thresholds corresponding to Figure 9.

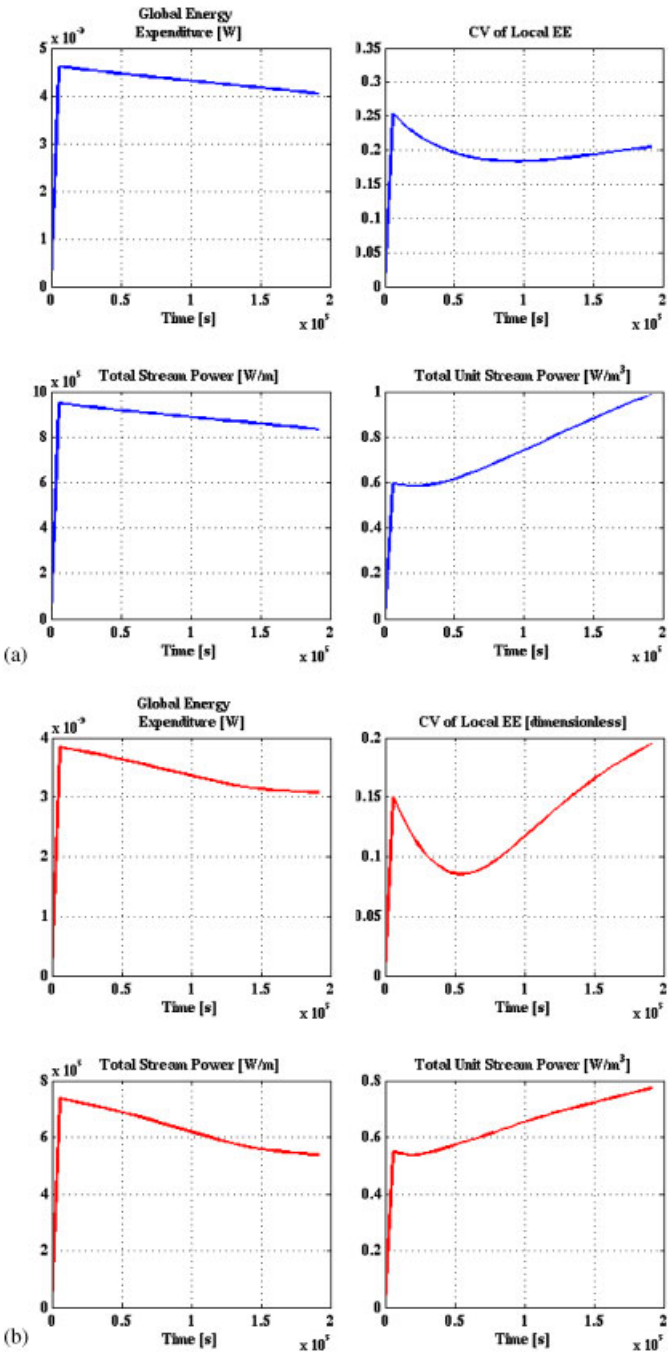

Figure 9. Energy characteristics (DD1): (a) threshold at $Q = 0.2$ [cm^3/s]; and (b) threshold at $Q = 1.0$ [cm^3/s].

Throughout these two-dimensional simulations, spatially heterogeneous flows develop with time and possess the characteristics expected of two-dimensional overland flow systems. Using the elevation matrix as a digital elevation model (not shown) and defining a network of micro-channels as all cells draining an upstream contributing area that exceeds a threshold, the simulations produce a network of channels that resembles networks observed in physical experiments [19].

Physical experiments conducted on artificial hillslopes, as described in Reference [19], develop equilibrium rill networks often in less than 5 h, but the time required for these rill networks to develop depends on the hillslope-scale slope. Qualitatively, the rates of development of the numerical model lag well behind the rates observed in the physical experiment. One possible explanation for this time lag of channel development is a lack of mass wasting mechanisms within the model for channel initiation and elongation. Mass wasting, specifically shallow landsliding, causes abrupt variations in the flow domain and topography (nick points) and leads to active rill development through upslope migration of the rill heads as observed during physical experiments and noted in the literature [27]. Also, distributions in soil infiltration characteristics as well as erodability, along with the distribution of rainfall on a much more discrete spatial domain, should add increased variability into the system and encourage two-dimensional heterogeneity. These simulations are computationally expensive and are the subject of ongoing research.

5. CONCLUDING REMARKS

This paper presents the mathematical development of a distributed, physically based, mechanistic hillslope hydrology model. The model consists of three components, each of which performs accurately when compared to known analytical solutions. The implementation of this model utilizes the most stable and accurate approaches developed for each algorithm individually, and implements some new stability controls on the coupled algorithm as a whole.

Two examples are presented to assess the ability of the model to capture interactions between overland flow, infiltration, and erosion and sediment transport. These examples show how the spatial distribution of rainfall rates, which leads to spatially distributed ponding time and overland flow depths and velocities, interacts with hillslope development and spatially distributed erosion. The model yields a description of hillslope evolution as well as flow and erosion rates under conditions where there are no mass wasting processes. An analysis of the energy expenditure characteristics of the flow indicates that this system of equations leads towards two-dimensional self-organization.

ACKNOWLEDGEMENTS

The authors gratefully acknowledge the financial support of the Center for Geosciences/Atmospheric Research through Cooperative Agreements DAAD19-01-2-0018 and DAAD19-02-2-0005 with the Army Research laboratory and of a National Science Foundation Trainee Grant (#9354864). The authors greatly appreciate the comments and suggestions of two anonymous reviewers of an earlier version of this manuscript. Their suggestions greatly improved this paper.

REFERENCES

1. Fiedler F, Ramírez JA. A numerical method for simulating discontinuous shallow flow over an infiltrating surface. *International Journal for Numerical Methods in Fluids* 2000; **32**:219–240.
2. Green WH, Ampt GA. Studies on soil physics, part I, the flow of air and water through soils. *Journal of Agricultural Science* 1931; **4**(1):1–24.
3. Richardson JR, Julien PY. Suitability of simplified overland flow equations. *Water Resources Research* 1994; **30**(3):665–671.
4. Emmett WW. The hydraulics of overland flow on hillslopes. *United States Geological Survey Professional Paper 662-A*, 1970.
5. Woolhiser DA. Simulation of unsteady overland flow. In *Unsteady Flow in Open Channels*, Mahmood K, Yevjevich V (eds), vol. 2. Water Resources Publications: Ft. Collins, CO, 1975.
6. Julien PY. *Erosion and Sedimentation*. Cambridge University Press: New York, NY, 1994.
7. Celia MA, Bouloutas ET, Zarba RL. A general mass-conservative numerical solution for the unsaturated flow equation. *Water Resources Research* 1990; **26**(7):1483–1496.
8. Paniconi C, Aldama AA, Wood EF. Numerical evaluation of iterative and noniterative methods for the solution of the nonlinear Richards equation. *Water Resources Research* 1991; **27**(6):1147–1163.
9. Rathfelder K, Abriola LM. Mass conservative numerical solutions of the head-based Richards equation. *Water Resources Research* 1994; **30**(9):2579–2586.
10. Zarba RL. A numerical investigation of unsaturated flow. *M.S. Thesis*, Department of Civil Engineering, M.I.T., Cambridge, 1998.
11. Press WH, Teukolsky SA, Vetterling WT, Flannery BP. *Numerical Recipes in Fortran 77*. Press Syndicate of the University of Cambridge, New York, 1986.
12. Kilinc M, Richardson EV. Mechanics of soil erosion from overland flow generated by simulated rainfall. *Hydrology Papers No. 63*, Colorado State University, 1972.
13. Chow VT, Maidment DR, Mays LW. *Applied Hydrology*. McGraw-Hill: New York.
14. Stoker JJ. 1957. *Water Waves*. Wiley: New York, NY, 1988.
15. Jha AK, Akiyama J, Ura M. First- and second-order flux difference splitting schemes for dam-break problem. *Journal of Hydraulic Engineering* 1995; **121**(12):877–884.
16. Philip JR. Theory of infiltration. *Advances in Hydroscience*, vol. 5. Academic Press: New York, 1957; **5**: 215–305.
17. Haverkamp R, Vauclin M, Touma J, Wierenga PJ, Vachaud G. A comparison of numerical simulation models for one-dimensional infiltration. *Soil Science Society of America Journal* 1977; **41**:285–294.
18. Knighton D. *Fluvial Forms & Processes*. Wiley: New York, 1998.
19. Raff DA, Ramírez JA, Smith JL. Hillslope drainage development with time, a physical experiment. *Geomorphology* 2004; **62**:169–180.
20. Ogden FL, Saghafian B. Green and Ampt infiltration with redistribution. *Journal of Irrigation and Drainage Engineering* 1997; **123**(5):386–393.
21. Yang CT. Potential energy and stream morphology. *Water Resources Research* 1971; **7**(2):311–323.
22. Chang HH. Geometry of gravel streams. *Journal of the Hydraulics Division* (ASCE) 1980; **106**(HY9): 1443–1456.
23. Langbein WB, Leopold LB. Quasi-equilibrium states in channel morphology. *American Journal of Science* 1964; **262**:782–794.
24. Carlston CW. Slope-discharge relations for eight rivers in the United States. *United States Geological Survey Professional Paper 600-D*, 1968; 45–47.
25. Molnar P, Ramírez JA. On downstream hydraulic geometry and optimal energy expenditure: case study of the Ashley and Taieri rivers. *Journal of Hydrology* 2002; **259**:105–115.
26. Rigon R, Rinaldo A, Rodriguez-Iturbe I, Bras RL, Ijjasz-Vasquez E. Optimal channel networks: a framework for the study of river basin morphology. *Water Resources Research* 1993; **29**(6):1635–1646.
27. Schumm SA, Mosley MP, Weaver WE. *Experimental Fluvial Geomorphology*. Wiley: New York, 1987.

